Front. Chem. Sci. Eng.
https://doi.org/10.1007/s11705-021-2066-6

RESEARCH ARTICLE

Advantageous mechanochemical synthesis of copper(I) selenide semiconductor, characterization, and properties

Katarína Gáborová[1,2], Marcela Achimovičová (✉)[1], Michal Hegedüs[3], Vladimír Girman[4], Mária Kaňuchová[5], Erika Dutková[1]

1 Institute of Geotechnics, Slovak Academy of Sciences, Košice 04001, Slovakia
2 Institute of Metallurgy, Faculty of Materials, Metallurgy and Recycling, Technical University, Košice 04201, Slovakia
3 Synthon, s.r.o., Blansko 67801, Czech Republic
4 Faculty of Science, Pavol Jozef Šafárik University, Košice 04154, Slovakia
5 Institute of Earth Resources, Faculty of Mining, Ecology, Process Control and Geotechnologies, Technical University, Košice 04200, Slovakia

Abstract Copper(I) selenide-nanocrystalline semiconductor was synthesized via one-step mechanochemical synthesis after 5 min milling in a planetary ball mill. The kinetics of synthesis was followed by X-ray powder diffraction analysis and specific surface area measurements of milled 2Cu/Se mixtures. The X-ray diffraction confirmed the orthorhombic crystal structure of Cu_2Se with the crystallite size ~25 nm. The surface chemical structure was studied by X-ray photoelectron spectroscopy, whereby the binding energy of the Cu 2p and Se 3d signals corresponded to Cu^+ and Se^{2-} oxidation states. Transmission electron microscopy revealed agglomerated nanocrystals and confirmed their orthorhombic structure, as well. The optical properties were studied utilizing ultraviolet-visible spectroscopy and photoluminescence spectroscopy. The direct bandgap energy 3.7 eV indicated a blue-shift phenomenon due to the quantum size effect. This type of Cu_2Se synthesis can be easily adapted to production dimensions using an industrial vibratory mill. The advantages of mechanochemical synthesis represent the potential for inexpensive, environmentally-friendly, and waste-free manufacturing of Cu_2Se.

Keywords Cu_2Se, berzelianite, nanocrystalline semiconductor, mechanochemical synthesis, planetary ball mill

1 Introduction

Copper selenides can exist in a wide range of compositions, both stoichiometric (CuSe, Cu_2Se, $CuSe_2$, Cu_3Se_2, Cu_7Se_4) and non-stoichiometric ($Cu_{2-x}Se$) [1]. Although they are rarely formed as minerals in nature, synthetic selenides represent a remarkable group of compounds with great potential in various scientific fields (such as: photovoltaics, thermoelectrics, or optoelectronics) due to their extraordinary electric and thermal properties [2–4]. Synthetic compounds derived from naturally occurring cubic berzelianite mineral ($Cu_{2-x}Se$, $x \approx 0.12$, *Fm-3m*, a = 5.879 Å), a *p*-type semiconductor, have been studied in detail through many different methods. Thus far, they have been synthesized through hydrothermal [5,6], heating-up process [7], solvothermal method [8], and facile chemical synthesis [9]. It was commonly reported that compounds of formula $Cu_{2-x}Se$ can exist in monoclinic low temperature (LT) β-$Cu_{2-x}Se$ phase or cubic high temperature (HT) α-$Cu_{2-x}Se$ phase with a transition around 400 K [3,10]. However, the latest study on the crystal structure of the LT phase revealed that the average structure is rather hexagonal (*R-3m*, a = 4.123 Å, c = 20.449 Å) [10]. Cu_2Se crystallizing in several crystal systems (i.e., orthorhombic, hexagonal, mixture monoclinic, and cubic) with different crystal morphologies (nanoparticles, nanotubes, nanowires, nanobelts, and nanosheets) have been prepared through sonochemical [11] or electrochemical synthesis [12], hot injection method [13], chemical reduction process [14], cation-exchange synthesis [15], and arc-melting process [2]. Although, the crystal structures reported by the authors are questionable, and are not unambiguously confirmed by the differences between X-ray patterns and their claims. For the $Cu_{2-x}Se$ fabrication, toxic chemicals were used (e.g., hydrazine), which are harmful to human health and the environment. Synthesis of Cu_2Se by milling-mechanochemical route represents a simple, one-pot, one-step, solvent-free, environmentally-friendly, and low-cost method at ambient pressure and temperature

Received February 2, 2021; accepted April 23, 2021

E-mail: achimovic@saske.sk

unlike the multi-step reaction processes which use toxic chemicals, organic solvents, HTs, and are time-consuming. The mechanochemical synthesis process can be easily up-scaled to industrial production in a large-capacity industrial mill, as well. These benefits represent the potential for inexpensive green manufacturing of Cu_2Se under essentially, waste-free conditions. Only recently in 2017, have Bulat and Ivanov with co-workers produced a single-phase material containing the α-Cu_2Se phase, after 2 h of milling in a high-energy ball mill, mainly studying its thermoelectric properties [16,17]. Li and co-workers synthesized almost single-phase β-$Cu_{2-x}Se$ after 20 min milling in a vibratory mill [18]; they discovered that continuous milling was more effective than intermittent milling, leading to a higher conversion degree. Moreover, a diffusion-controlled solid-state reaction mechanism was proposed for the mechanochemical synthesis of $Cu_{2-x}Se$; however, the thermodynamic aspect of the reaction, the morphology, the size, and the shape of mechanochemically synthesized Cu_2Se nanocrystals, as well as the optical properties, were not investigated until now.

In the present study, nanostructured copper selenide Cu_2Se was prepared in a high-energy planetary ball mill at ambient temperature and pressure through the short and one-step process of mechanochemical synthesis. The course and mechanism of mechanochemical synthesis, the crystal structure, the morphology, and the physical and optical properties of the product were investigated.

2 Experimental

2.1 Mechanochemical synthesis

Mechanochemical synthesis of Cu_2Se was performed by co-milling of copper ($>99.7\%$, 54.02 μm, Pometon GmbH, Germany) and selenium powders (99.5%, 74 μm, Aldrich, Germany) in the planetary ball mill Pulverisette 6 (Fritsch, Germany), according to the reaction:

$$2Cu + Se = Cu_2Se \quad (1)$$

The reaction is thermodynamically feasible due to the negative value of enthalpy change $\Delta H^0_{298} = -65.31$ $kJ \cdot mol^{-1}$. The following milling conditions were used: loading of 50 mill balls (10 mm in diameter), the material of the milling chamber and balls-WC, the volume of the milling chamber is 250 mL, 3.08 g Cu powder, 1.92 g Se powder, ball-to-powder ratio 73:1, milling atmosphere-Ar, rotation speed is 550 $r \cdot min^{-1}$, and milling time 0.5–7 min. The course of the mechanochemical synthesis was monitored *in situ* by the planetary ball mill Pulverisette 7 Premium line with a special milling chamber equipped with a sensor for monitoring gas and temperature changes during the milling process — EASY GTM system (Fritsch, Germany). The milling conditions were as follows: loading of 15 mill balls (10 mm in diameter), the material of the milling chamber and balls-WC, the volume of the milling chamber is 80 mL, 0.9856 g Cu powder, 0.6144 g Se powder, ball-to-powder ratio 73:1, milling atmosphere-air, rotation speed is 550 $r \cdot min^{-1}$, and milling time 5 min.

2.2 Characterization techniques

The X-ray powder diffraction patterns (XRPD) of the samples were measured with a Panalytical Empyrean diffractometer working in θ–2θ Bragg Brentano geometry equipped with a CuK$\alpha_{1,2}$ X-ray source (0.154439 nm) at 40 kV and 40 mA. Fixed divergence slit (1/4°), anti-scatter slit (1/2°), 10 mm mask, and 0.02 rad Soller slit were used for the incident beam path. The pattern was measured in the 2θ range of 10°–100° with a step size of 0.027°, and a step time of 450 s. During measurement, the sample was revolved at 30 $r \cdot min^{-1}$. The data were analyzed utilizing JANA2006 and HighScore Plus software. The pseudo-Voigt function was used to model diffraction lines. The JCPDS PDF database was utilized for phase identification.

The specific surface area (S_A) measurements were determined by the low-temperature nitrogen adsorption method in a Gemini 2360 sorption apparatus (Micromeritics, USA).

Particle size distribution analysis (PSD) was performed by a laser diffraction system using Mastersizer 2000E particle size analyzer (Malvern Pananalytical, UK) with dry feeder Scirocco 2000M and measuring range 0.02–2000 μm.

X-ray photoelectron spectroscopy (XPS) of samples was performed using XPS instrument SPECS, equipped with a hemispherical energy analyzer PHOIBOS 100 SCD and a non-monochromatic X-ray source. The survey surface spectrum was measured at 70 eV pass energy and core spectra at 20 eV at room temperature. All spectra were acquired at a basic pressure of 1×10^{-8} mbar with AlKα excitation at 10 kV (200 W).

Scanning electron microscopy (SEM) study was performed using a MIRA3 FE-SEM (field emission scanning electron microscopy) microscope (TESCAN, Czech Republic) equipped with the energy-dispersive X-ray (EDX) detector (Oxford Instrument, UK).

Transmission electron microscopy (TEM) observations were carried out using a JEOL 2100F UHR microscope equipped with the Schottky field emission source and operated at 200 kV. The images were taken in high-resolution mode and for structure identification, the selected area diffraction was used. Regarding electron diffraction experiments, the microscope was precisely calibrated using MoO_3 crystal; the gold nanoparticles were used for confirmation. Both samples were dispersed in pure ethanol, and were ultrasonicated for 10 min to reduce the agglomeration effect of crystals. Drops of the solutions were put on the conventional copper support grid, covered with flat carbon film. Subsequently, the samples were stored in a vacuum to eliminate ethanol.

The optical absorption (ultraviolet-visible spectroscopy (UV-Vis)) spectrum was collected using the spectrophotometer Helios Gamma (Thermo Electron Corporation, Great Britain) in the range of 200–900 nm. The powder sample (5 mg) was dispersed in 5 mL of 96% ethanol (Centralchem, Slovakia) by ultrasonic stirring for 10 min. The absorbance spectra were measured in a quartz cell. Photoluminescence (PL) spectra were measured over a wavelength ranging from 500 to 800 nm, by photon counting spectrofluorometer PC1 (ISS, USA) with an excitation wavelength of 480 nm. A 300 W xenon lamp was used as the excitation source. Excitation and emission slit widths were set 1 and 2 mm. One-cm path length rectangular quartz cuvette was used. The PL intensity was measured from the Cu_2Se powder ultrasonically dispersed in absolute ethanol.

3 Results and discussion

The XRPD patterns of 2Cu/Se mixtures milled for times 0.5–5 min are given in Fig. 1. The pattern of the mixture milled for 0.5 min shows the peaks of unreacted elemental Cu (JCPDS PDF 4-0836) and Se (JCPDS PDF 1-0853). Despite the extremely short milling time, the reaction progress is obvious. The formation of Cu_3Se_2 (JCPDS PDF 65-1656) as an intermediate phase is also observed.

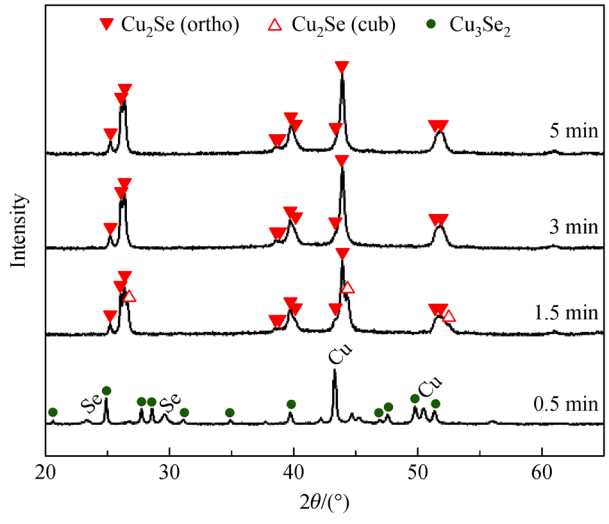

Fig. 1 XRPD patterns of 2Cu/Se mixtures milled for 0.5, 1.5, 3, and 5 min.

Thus, the mechanochemical reaction from elemental precursors is indirect and proceeds via two steps. According to several studies, the coexistence of Cu_2Se and Cu_3Se_2 phase can be observed in Cu/Se system [7,19]. By increasing milling time up to 1.5 min, the peaks assigned Cu, Se, and Cu_3Se_2 vanish completely. On the contrary, diffraction peaks corresponding to the orthorhombic Cu_2Se phase (JCPDS PDF 47-1448) can be identified. Additional peaks appearing at angles close to the main diffractions of orthorhombic Cu_2Se point to the possible formation of a mixture of two Cu_2Se products with different symmetry — cubic and orthorhombic. Further increase in the milling time shifts the reaction towards the orthorhombic phase. After 5 min of milling, no changes to the phase composition of the prepared samples can be detected. A gradual broadening of the diffraction peaks, resulting from crystallite size reduction, is only observed if the milling time is increased. Based on the obtained results the following reaction scheme was suggested:

$$4Cu + 2Se \rightarrow Cu_3Se_2 + Cu \rightarrow Cu_2Se(cub) + Cu_2Se(ortho) \rightarrow 2Cu_2Se(ortho) \quad (2)$$

This is in accordance with the gradual incorporation of copper atoms into the crystal lattice. The cubic Cu_2Se (JCPDS PDF 76-0136) is supposed to form first and is rapidly transformed into the orthorhombic phase. This also proves the mechanochemical approach to be a powerful tool for polymorphic control. Nonetheless, further study is needed to understand the behavior of the Cu/Se system exposed to neat milling technique.

An in-depth analysis of the pattern of the sample milled for 5 min was performed. Even though the cubic structure (space group *Fm-3m*, $a \approx 0.575$ nm) is most common for a wide range of non-stoichiometric composition of $Cu_{2-x}Se$, other structures have been reported as well-monoclinic, orthorhombic, tetragonal, or hexagonal. The cubic structure, also known as the HT α-$Cu_{2-x}Se$ is metastable, and it transforms very slowly to the LT phase [19]. Only recently has the crystal structure of the LT β-$Cu_{2-x}Se$ phase been revised by Eikeland et al. [10]. Their exhaustive study proved that the average structure of the LT β-$Cu_{2-x}Se$ phase is not monoclinic, but rather rhombohedral [3,10]. Still, the assignment of the structure of the prepared samples remains a challenge. Mostly polycrystalline samples of $Cu_{2-x}Se$ with crystallite size in the nanometer range are prepared, which makes it hard to assign the correct structure, especially for lower symmetry crystal systems. To our knowledge, only crystalline structures of LT-$Cu_{2-x}Se$ and HT-$Cu_{2-x}Se$ were fully determined. The assignment of the structure is further complicated by the possible co-existence of the phases (cubic and orthorhombic), as well as the presence of possible impurity phases (Cu_3Se_2 observed as an intermediate product, Cu_2O, or even CuO as oxidation by-products) [19,20]. When comparing our pattern with the database data, we found that it matches the best orthorhombic structure (JCPDS PDF 47-1448) reported several times before for the samples prepared hydrothermally or electrochemically [20–22]. The LeBail refinement was performed starting with the cell parameters reported in the work of Haram

et al. [22]. The XRPD pattern in Fig. 2 could be easily indexed to the orthorhombic structure (see Table 1). The following cell parameters were obtained based on the least-square refinement results: a = 1.3856 nm, b = 2.0494 nm, c = 0.3923 nm (statistics of the refinement along with the graphical output is given in Fig. 2). The average crystallite size was determined to be 25 nm. Some impurity phases might be present in trace amounts, but their detection is precluded by relatively high background and strong overlap of the reflections.

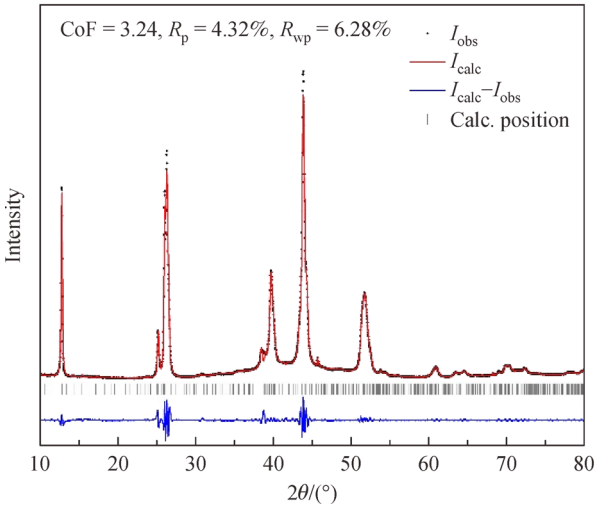

Fig. 2 The graphical LeBail refinement output of the orthorhombic cell parameters against measured data of 2Cu/Se mixtures milled for 5 min.

The EASY GTM system was used to monitor the mechanochemical synthesis of Cu_2Se *in situ*. Figure 3(a) shows the course of the reaction as a function of temperature and gas pressure during 5 min milling of the stoichiometric mixture 2Cu/Se. The temperature of the reaction increased by only 0.1 °C after 0.5 min, while the gas pressure was also not directly proportional to the increasing milling time in the range of 0.5 to 2 min. After a certain reaction phase, corresponding to a milling time of ~2 min, the change in gas pressure is constant, which is likely correlated to the completed formation of the Cu_2Se product — a mixture of Cu_2Se (cub) and Cu_2Se (ortho) phases, which already occured during the milling time of 1.5 min. During the experiment, neither a sharp increase in temperature or gas pressure was observed. Such a gradual course of the mechanochemical reaction is contradictory to the finding of Baláž et al. who observed explosive character of the reaction leading to analogous compound Cu_2S using the same Cu-powder precursor [23]; the difference between the reaction enthalpy of Cu_2S (–79.5 $kJ \cdot mol^{-1}$) and Cu_2Se is only –14.19 $kJ \cdot mol^{-1}$, as well. The different behavior of the reaction mixture can be closely connected to the reaction mechanism, where in the case of Cu-Se system, Cu_3Se_2 product is first formed and then subsequently transformed into Cu_2Se. Despite no significant changes, neither in temperature nor pressure during the reaction, the formation of the Cu_2Se phase (JCPDS PDF 47-1448) is confirmed by the pattern in Fig. 3(b), which corresponds to the comparable product previously obtained and illustrated in Fig. 2. Additionally, there are visible peaks belonging to tungsten carbide WC (JCPDS PDF 03-1096), which comes from the wear of the milling chamber and milling media.

S_A dependence of milled 2Cu/Se mixtures on the time of mechanochemical synthesis is demonstrated in Fig. 4. The hyperbolic dependence differs from dependences already reported in literature dealing with the mechanochemical synthesis of Pb, Zn, Bi, and Co selenides [24–27]. S_A of 2Cu/Se mixtures decreased with time of mechanochemical synthesis, reaching a value of 0.23 $m^2 \cdot g^{-1}$ for 5 min milled and a minimum value of 0.14 $m^2 \cdot g^{-1}$ for 7 min milled Cu_2Se products. This means that already in the initial stage of milling, the particles of the reaction precursors aggregate, and the subsequent rapid formation of the reaction product in the form of agglomerates is also evident from SEM images later shown.

PSD curves of the Cu_2Se products in Fig. 5 confirmed this result as well. The mean particle size calculated from PSD analysis $d(0.5)$ = 42.67 μm for Cu_2Se milled for 5 min and $d(0.5)$ = 70.69 μm for Cu_2Se milled for 7 min, revealed that they are also affected by the mechanochemical synthesis time; with increasing milling time, the particle size of the products increases and their specific surface area decreases.

XPS analysis, a method for the study of the chemical structure of the surface layers of material, has evidenced the changes of the valence states for copper, as well as selenium in mechanochemically synthesized Cu_2Se. The detailed XPS spectral lines of Cu 2p and Se 3d core levels are shown in Fig. 6. The binding energy (BE) values 932.1 and 952.1 eV (see Fig. 6(a)) correspond to the Cu $2p_{3/2}$ and Cu $2p_{1/2}$ spectral lines of Cu^+ species [2,28]. However, the presence of a satellite peak assigned to Cu^{2+} with BE of around ~940–943 eV, suggests slight surface oxidation of the product. This is further proved by an asymmetry of XPS lines and the strong overlap of Cu^{2+}/Cu^+ signals. The signals could be assigned to possible CuO surface impurity or Cu^{2+} specimens in copper-deficient $Cu_{2-x}Se$ compound [2,6]. According to the work of Riha et al., Cu^+ in Cu_2Se oxidizes to Cu^{2+} when exposed to air and the process can be accelerated in the case of nanoparticles with a high density of surface sites [29]. Surface oxidation was observed before for mechanochemically synthesized copper sulfides as well, where the formation of CuO was reported [30,31]. Surface oxidation was also observed in the case when the product was stored directly after synthesis under argon gas. In Fig. 6(b) the peaks with BE values 54.0 eV for Se $3d_{5/2}$ and 54.9 eV for Se $3d_{3/2}$ belong to the prepared Cu_2Se product, and the valence of Se responds to Se^{2-} species followed by references [32,33].

Table 1 Indexing of the orthorhombic unit cell along with the relative intensity of Bragg reflections

h	*k*	*l*	*d*/nm calc.*	I/I_0	*d*/nm obs.
2	0	0	0.6928	9.5	0.6910
0	3	0	0.6831	78.7	0.6860
2	5	0	0.3528	20.4	0.3523
0	6	0	0.3416	78.1	0.3417
2	1	1	0.3367	88.1	0.3378
0	7	1	0.2346	4.4	0.2323
4	4	1	0.2316	0.0	–
0	9	0	0.2277	27.0	0.2269
6	2	0	0.2253	11.8	0.2250
3	7	1	0.2092	100.0	0.2083
5	4	1	0.2070	63.1	0.2065
3	2	2	0.1778	20.5	0.1777
7	0	1	0.1767	26.6	0.1768
4	0	2	0.1707	1.6	0.1703
4	2	2	0.1684	0.6	0.1685
9	1	0	0.1535	2.2	0.1528
9	2	0	0.1522	4.4	0.1520
9	4	0	0.1474	1.9	0.1468
7	3	2	1.365	3.0	0.1361
0	0	3	1.308	2.5	0.1306

*calculated values from refined cell parameters a = 1.3856 nm, b = 2.0494 nm, c = 0.3923 nm.

Figure 7 shows the SEM micrographs of the starting reagents. Copper powder exhibits the typical morphology of the metal prepared by electrolysis. This type of copper morphology has previously been shown to be highly reactive. On the other hand, selenium powder showed substantially bigger round-shaped agglomerates of particles. The morphology of the milled mixtures for 0.5, 1.5, and 5 min supports findings both from XRPD analysis and the activated surface area determination. Even after 0.5 min of milling, the overall morphology of the mixture changes significantly, which supports fast conversion of elemental precursors. Unreacted copper metal, also detected by XRPD analysis, can be seen in Fig. 7(c) inset as detected by EDX analysis (shown in red color). This could be identified also based on its original morphology. The Cu_3Se_2 intermediate product revealed by XRPD could not be satisfactorily spotted by EDX analysis. In the final product after 5 min of milling, no unreacted metals were found. An increase in the particle size is, however, noticeable and in good accordance with provided PSD analysis. The average at% composition from the selected area (Fig. 7(d) inset) was found to be slightly higher than calculated. This deviation is most likely caused by the rough surface of the sample and therefore, by the uncertainty of elemental composition determination.

In Fig. 8, detailed structure and morphology of the Cu_2Se product detected by TEM are presented. The powder particles are not monocrystalline and consist of many agglomerated nanocrystals (Fig. 8(a)). In Fig. 8(b), one of the particles is imaged at the high-resolution and reveals atomic interplanar distances. The estimated size of nanocrystallites is on the level of tens of nanometers. Diffraction patterns were processed by radial integration and for refinement, the calibrated correction coefficients were used. These corrections are necessary to compensate for instrumental diffraction error, which makes the diffraction data more accurate. Obtained reflections of the diffraction pattern perfectly fit the orthorhombic structure of the Cu_2Se phase with lattice parameters a = 1.4103 nm, b = 2.0402 nm, and c = 0.4133 nm. These cell parameters are close to the values calculated based on the LeBail refinement of XRPD data. All visible reflections on the selected area diffraction pattern were measured, however, to better readability only a few of them were labeled in Fig. 8(c).

Cu_2Se is a *p*-type of semiconductor with different values of a direct bandgap in the range 1.31–3.4 eV depending on particle size, crystal structure, phase purity, method of preparation, and other factors [34]. The optical bandgap energy of mechanochemically synthesized Cu_2Se was obtained based on the recorded absorption spectrum in the UV-Vis spectral region showed in Fig. 9. The energy bandgap can be determined using Tauc's relation for direct allowed electronic transitions from the valence to the

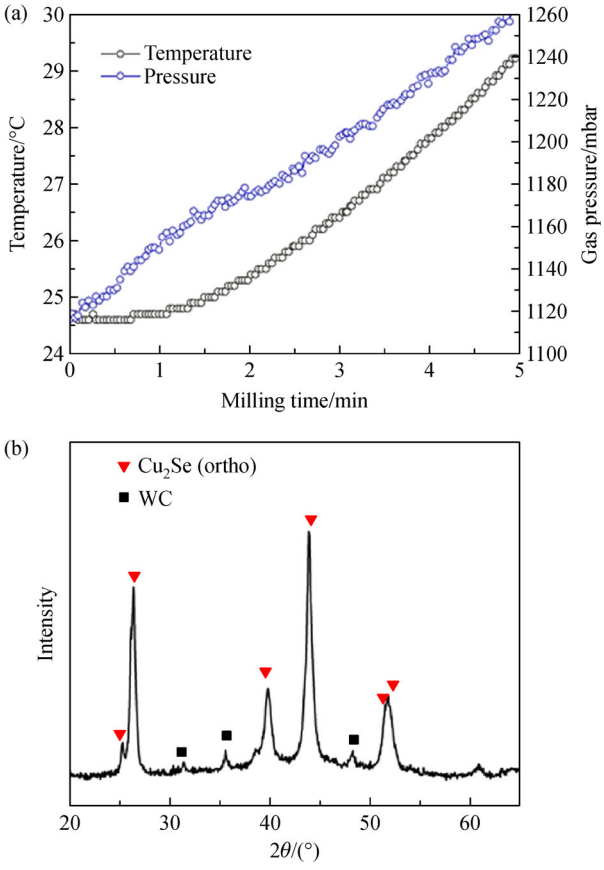

Fig. 3 *In-situ* monitoring of Cu_2Se mechanochemical synthesis: (a) gas pressure and temperature changes during milling; (b) XRPD pattern of 2Cu/Se mixture milled for 5 min.

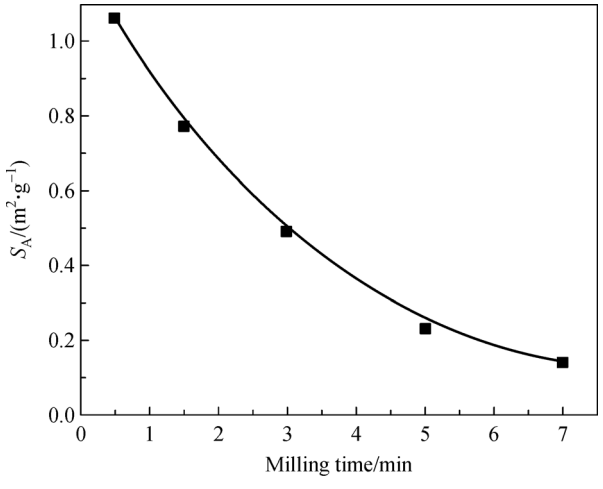

Fig. 4 Specific surface area, S_A of milled 2Cu/Se mixtures *vs.* time of mechanochemical synthesis, t_M.

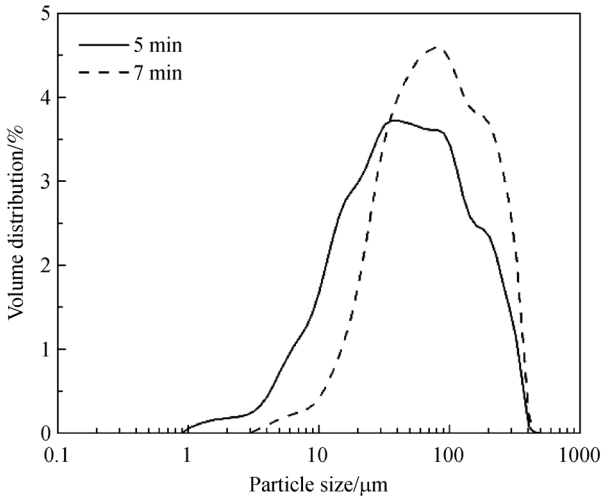

Fig. 5 PSD curves of 2Cu/Se mixtures milled for 5 and 7 min.

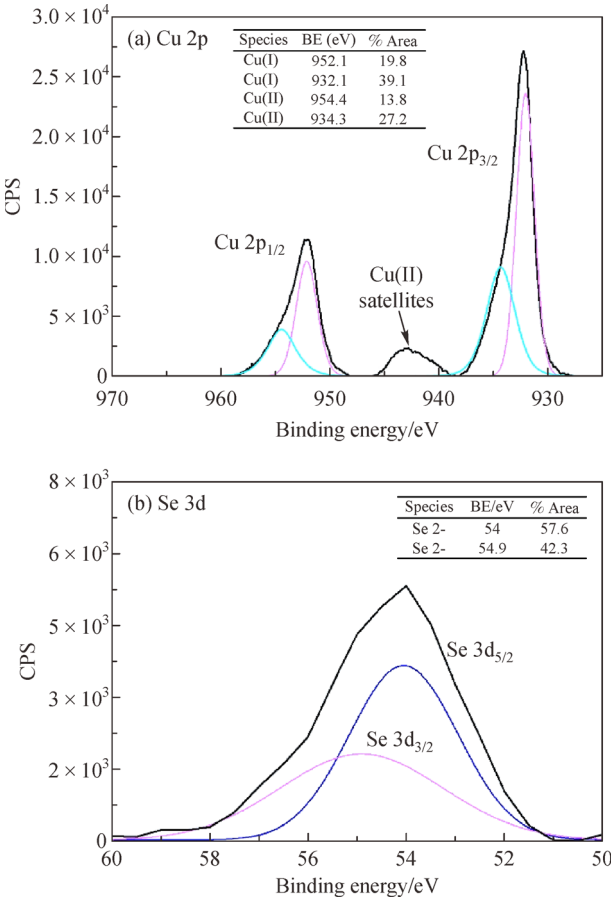

Fig. 6 XPS spectra of mechanochemically synthesized Cu_2Se: (a) Cu 2p; (b) Se 3d.

conduction band [35]. From the linear trend of the $(\alpha h\nu)^2$ *versus* hν dependence in the inset of Fig. 8, the value of bandgap energy 3.7 eV is determined. The higher bandgap value of mechanochemically synthesized Cu_2Se against the fundamental direct bandgap of bulk copper selenide (~2.4 eV) indicates a blue-shift phenomenon, due to the quantum size effect [28]. This effect can be attributed to the

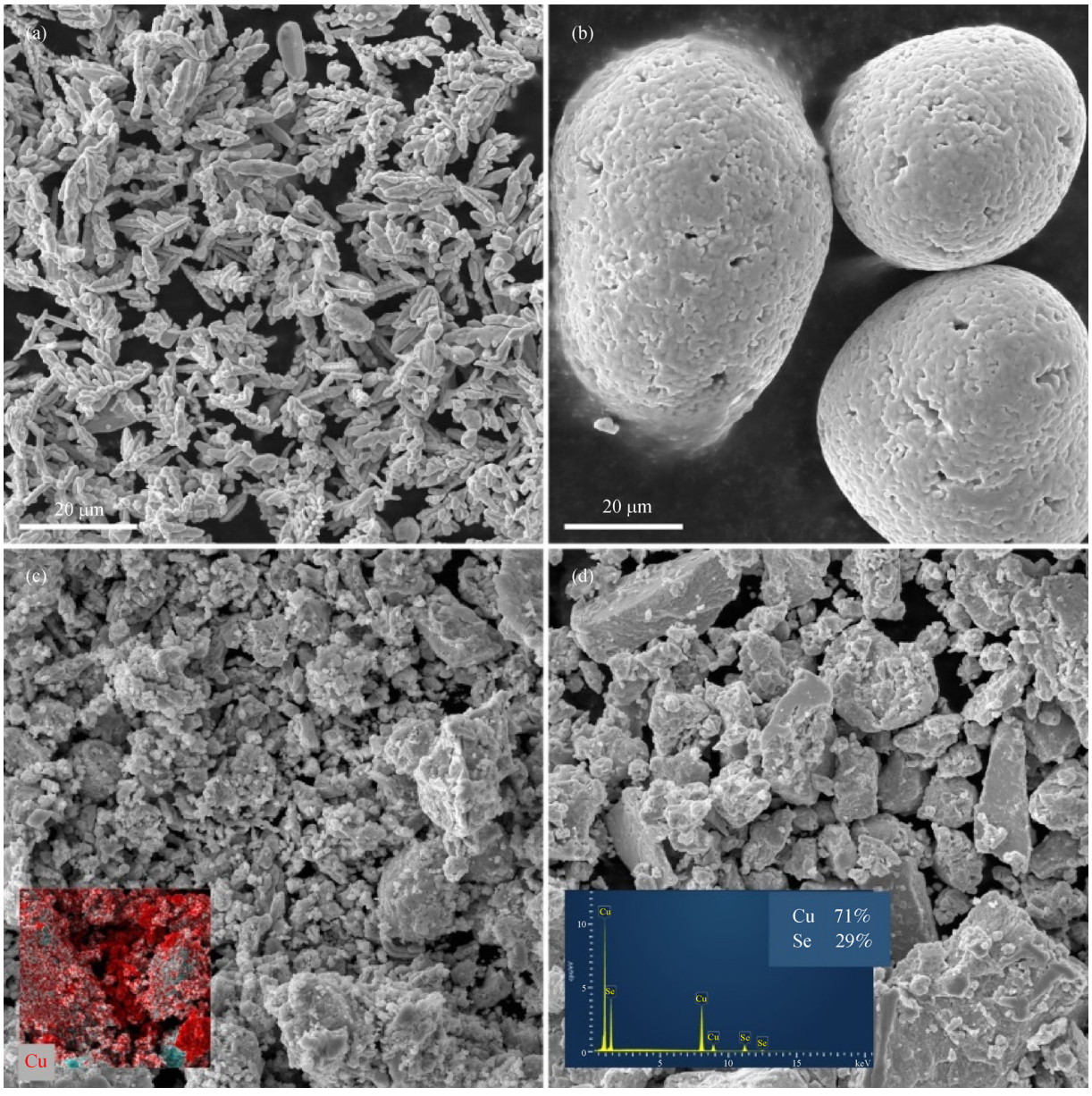

Fig. 7 SEM micrographs of starting reagents: (a) elemental copper and (b) selenium at the same magnification with milled mixtures for (c) 0.5 min and (d) 5 min.

existence of very small nanoparticles agglomerated into the big clusters and may be conditioned by chemical features of copper with the easy occurrence of multivalent states [36]. No data on the optical bandgap of Cu_2Se prepared by mechanochemical synthesis is available in the literature for comparison.

The optical properties of the mechanochemically synthesized Cu_2Se were also studied by using PL spectroscopy. The room temperature PL spectrum of Cu_2Se with an exciting wavelength at 480 nm (2.56 eV) is presented in Fig. 10. It can be seen from the spectrum that two weak peaks are observed at 522 and 550 nm. The peak situated at 522 nm (2.36 eV) may be attributed to the defect-related emission due to copper vacancies and interstitials defects related to the mechanochemically synthesized sample [37]. It is assumed that all defects in nanocrystals may be generated as a consequence of high-energy milling. The weak peak positioned at 550 nm (2.24 eV) may originate from defects of Se or Cu. It is in accordance with the data reported in the paper [38].

4 Conclusions

Simple and fast mechanochemical synthesis of nanostructured Cu_2Se from elemental copper and selenium by

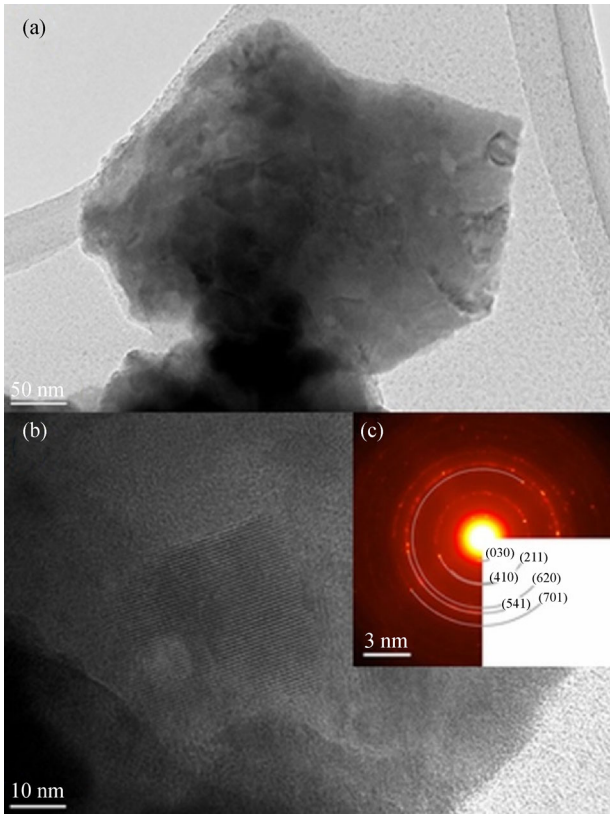

Fig. 8 TEM images of (a) agglomerated crystals of Cu_2Se after 5 min of mechanochemical synthesis; (b) detail of Cu_2Se particle imaged at magnification 300 kx; (c) selected area electron diffraction (SAED) pattern of the same crystals.

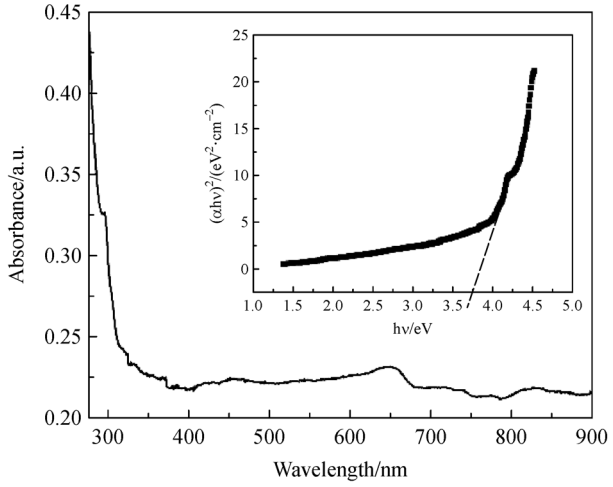

Fig. 9 UV-Vis optical absorption spectrum of Cu_2Se after 5 min of mechanochemical synthesis (Inset: $(\alpha h\nu)^2$ *vs.* hν plot and the obtained bandgap energy 3.7 eV).

high-energy milling in one-step is reported herein. The XRPD analysis confirmed that mechanochemical synthesis

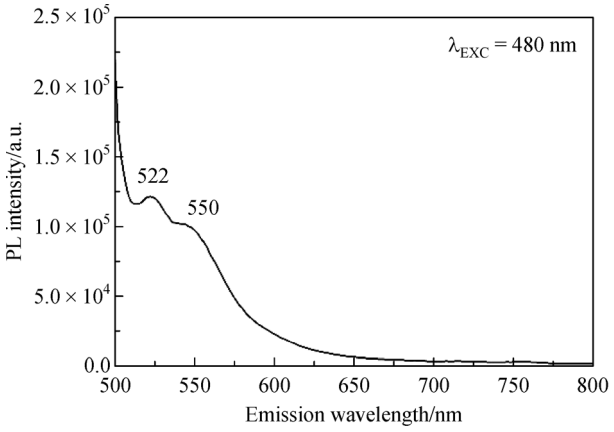

Fig. 10 PL spectrum of Cu_2Se product at an excitation wavelength of 480 nm.

is completed after 5 min of milling and determined the average crystallite size of Cu_2Se was 25 nm. The course of synthesis controlled by the GTM system revealed a gradual process without a sharp increase in temperature or gas pressure. The reaction mechanism of the synthesis can be described with the proposed reaction scheme. The mean particle size of Cu_2Se products increased with increasing milling time and their S_A decreased. The orthorhombic crystal structure of Cu_2Se was additionally confirmed by TEM and SAED analysis, which also showed agglomerated nanocrystals with a diameter of 500 nm and larger. XPS analysis proved the oxidation state of Cu^+ and Se^{2-} on the surface of Cu_2Se, but also showed slight oxidation of surface copper. UV-Vis measurements were used for the determination of the energy band gap of 3.7 eV, which indicated direct optical transition in Cu_2Se semiconductor. The higher bandgap value of mechanochemically synthesized Cu_2Se against the bulk copper selenide (~2.4 eV) indicates a blue-shift phenomenon due to the quantum size effect. In our work, we demonstrated that the mechanochemical synthesis is a rapid, environmentally-friendly, and relatively low-cost process for the preparation of nanostructured Cu_2Se semiconductor at ambient temperature, thusly representing a suitable alternative to the existing methods of Cu_2Se production. From our previous research and experience, it is evident that this type of synthesis can be easily adapted to production dimensions using an industrial vibratory mill.

Acknowledgements This work was realized within the frame of the project "Research Centre of Advanced Materials and Technologies for Recent and Future Applications PROMATECH", ITMS 26220220186, supported by the Operational Program "Research and Development" financed through European Regional Development Fund, Slovak Research and Development Agency under the contract No. APVV-18-0357, and by the Slovak Grant Agency VEGA (projects 02/0065/18, 02/0103/20). We would like to thank Professor J. Briančin for SEM observations, and the native speaker Mrs. Ch. Dejanakul-Wolfe for the formal text revision.

References

1. Heydin R D, Murray R M. The crystal structures of $Cu_{1.8}Se$, Cu_3Se_2, α- and γ-CuSe, $CuSe_2$, and $CuSe_2$II. Canadian Journal of Chemistry, 1976, 54(6): 841–848
2. Butt S, Farooq M, Mahmood W, Salam S, Sultan M, Basit M, Ma J, Lin Y, Nan C. One-step rapid synthesis of Cu_2Se with enhanced thermoelectric properties. Journal of Alloys and Compounds, 2019, 786: 557–564
3. Gulay L, Daszkiewicz M, Strok O, Pietraszko A. Crystal structure of Cu_2Se. Chemistry of Metals and Alloys, 2011, 4(3/4): 200–205
4. Byeon D, Sobota R, Delime-Codrin K, Choi S, Hirata K, Adachi M, Kiyama M, Matsuura T, Yamamoto Y, Matsunami M, Takeuchi T. Discovery of colossal Seebeck effect in metallic Cu_2Se. Nature Communications, 2019, 10(1): 72
5. Liu K, Liu H, Wang J, Shi L J. Synthesis and characterization of Cu_2Se prepared by hydrothermal co-reduction. Journal of Alloys and Compounds, 2009, 484(1-2): 674–676
6. Han X, Liao F, Zhang Y, Yuan Z, Chen H, Xu C. CTAB-assisted hydrothermal synthesis of Cu_2Se films composed of nanowire networks. Materials Letters, 2018, 210: 62–65
7. Hsiang H, Hsu W, Lu L, Chang Y, Yen F. Cuprous selenide nanocrystal synthesis and characterization. Materials Research Bulletin, 2013, 48(2): 715–720
8. Jia F, Zhang S, Zhang X, Peng X, Zhang H, Xiang Y. Sb-triggered β-to-α transition: solvothermal synthesis of metastable alpha-Cu_2Se. Chemistry (Weinheim an der Bergstrasse, Germany), 2014, 20(48): 15941–15946
9. Zhao Y, Zhu L, Jiang Y, Xie H, Zhang G, Ba N. Microphone shaped Cu_2Se micro/nanoarchitecture: preparation, formation mechanism and optical property. Materials Letters, 2015, 147: 82–84
10. Eikeland E, Blichfeld A, Borup K, Zhao K, Overgaard J, Shi X, Chen L, Iversen B. Crystal structure across the beta to alpha phase transition in thermoelectric $Cu_{2-x}Se$. Journal of Applied Crystallography, 2017, 4: 476–485
11. Xu S, Wang H, Zhu J, Chen H. Sonochemical synthesis of copper selenides nanocrystals with different phases. Journal of Crystal Growth, 2002, 234(1): 263–266
12. Kaur H, Kaur J, Singh L, Singh S. Electrochemical synthesis and characterization of Cu_2Se nanowires. Superlattices and Microstructures, 2013, 64: 294–302
13. Yang C, Hsiang H, Tu J. Copper selenide crystallites synthesized using the hot-injection process. Advanced Powder Technology, 2016, 27(3): 959–963
14. Yang C, Hsiang H. Rapid synthesis and characterization of nearly dispersed marcasite $CuSe_2$ and berzelianite Cu_2Se crystallites using the chemical reduction process. Materials Research Bulletin, 2018, 97: 30–36
15. Su Y, Li G, Guo Z, Li Y Y, Li Y X, Huang X J, Liu J H. Cation-exchange synthesis of Cu_2Se nanobelts and thermal conversion to porous CuO nanobelts with highly selective sensing toward H_2S. ACS Applied Nano Materials, 2018, 1(1): 245–253
16. Bulat L, Osvenskii V, Ivanov A, Sorokin A, Pshenay-Severin D, Bublik V, Tabachkova N, Panchenko V, Lavrentev M. Experimental and theoretical study of the thermoelectric properties of copper selenide. Semiconductors, 2017, 51(7): 854–857
17. Ivanov A, Sorokin A, Panchenko V, Tarasova I, Tabachkova N, Bublik V, Akchurin R. Structure of the Cu_2Se compound produced by different methods. Semiconductors, 2017, 51(7): 866–869
18. Li J, Liu G, Wu X, He G, Yang Z, Li J. Reaction mechanism in mechanochemical synthesis of $Cu_{2-x}Se$. Ceramics International, 2018, 44(18): 22172–22175
19. Stevels A, Jellinek F. Phase transitions in copper chalcogenides: 1. Copper-selenium system. Recueil Des Travaux Chimiques Des Pays-Bas, 1971, 90(3): 273–283
20. Lévy-Clément C, Neumann-Spallart M, Haram S, Santhanam K. Chemical bath deposition of cubic copper(I) selenide and its room temperature transformation to the orthorhombic phase. Thin Solid Films, 1997, 302(1-2): 12–16
21. Kopp O, Cavin O. Hydrothermal growth of single-crystal Cu_2Se (Berzelianite). Journal of Crystal Growth, 1984, 67(2): 391–392
22. Haram S, Santhanam K, Neumann-Spallart M, Lévy-Clément C. Electroless deposition on copper substrates and characterization of thin-films of copper(I) selenide. Materials Research Bulletin, 1992, 27(10): 1185–1191
23. Baláž M, Zorkovská A, Urakaev F, Baláž P, Briančin J, Bujňáková Z, Achimovičová M, Gock E. Ultrafast mechanochemical synthesis of copper sulfides. RSC Advances, 2016, 6(91): 87836–87842
24. Achimovičová M, Daneu N, Rečnik A, Ďurišin J, Peter B, Fabián M, Kováč J, Šatka A. Characterization of mechanochemically synthesized lead selenide. Chemical Papers, 2009, 63(5): 562–567
25. Achimovičová M, Baláž P, Ohtani T, Kostova N, Tyuliev G, Feldhoff A, Šepelák V. Characterization of mechanochemically synthesized ZnSe in a laboratory and an industrial mill. Solid State Ionics, 2011, 192(1): 632–637
26. Achimovičová M, Gotor F, Real C, Daneu N. Mechanochemical synthesis and characterization of nanocrystalline BiSe, Bi_2Se_3 semiconductors. Journal of Materials Science Materials in Electronics, 2012, 23(10): 1844–1850
27. Achimovičová M, Daneu N, Tóthová E, Mazaj M, Dutková E. Combined mechanochemical/thermal annealing approach for the synthesis of Co_9Se_8 with potential optical properties. Applied Physics. A, Materials Science & Processing, 2019, 125(1): 8
28. Zhu L, Xie H, Liu Y, Chen D, Bian M, Zheng W. Novel ultralong hollow hyperbranched $Cu_{2-x}Se$ with nanosheets hierarchical structure: preparation, formation mechanism and properties. Journal of Alloys and Compounds, 2019, 802: 430–436
29. Riha S, Johnson D, Prieto A. Cu_2Se nanoparticles with tunable electronic properties due to a controlled solid-state phase transition driven by copper oxidation and cationic conduction. Journal of the American Chemical Society, 2011, 133(5): 1383–1390
30. Baláž M, Dutková E, Bujňáková Z, Tóthová E, Kostova N, Karakirova Y, Briančin J, Kaňuchová M. Mechanochemistry of copper sulfides: characterization, surface oxidation and photocatalytic activity. Journal of Alloys and Compounds, 2018, 746: 576–582
31. Hegedüs M, Baláž M, Tešinský M, Sayagues M, Siffalovic P, Kruľaková M, Kaňuchová M, Briančin J, Fabián M, Baláž P. Scalable synthesis of potential solar cell absorber Cu_2SnS_3 (CTS) from nanoprecursors. Journal of Alloys and Compounds, 2018, 768: 1006–1015
32. Tufts B J, Abrahams I L, Caley C E, Lunt S R, Miskelly G M, Sailor

M J, Santangelo P G, Lewis N S, Roe A L, Hodgson A O. XPS and EXAFS studies of the reactions of Co(III) ammine complexes with GAAS-surfaces. Journal of the American Chemical Society, 1990, 112(13): 5123–5136

33. Theye M L, Gheorghiu A, Senemaud C H, Kotkata M F, Kandil K. Studies of short-range order in amorphous Ge_xSe_{100-x} compounds by X-ray photoelectron spectroscopy. Philosophical Magazine B, Physics of Condensed Matter. Structural, Electronic, Optical and Magnetic Properties, 1994, 69: 209–222
34. Zyoud A, Murtada K, Kwon H, Choi H, Kim T, Helal M, Faroun M, Bsharat H, Park D, Hilal H. Copper selenide film electrodes prepared by combined electrochemical/chemical bath depositions with high photo-electrochemical conversion efficiency and stability. Solid State Sciences, 2018, 75: 53–62
35. Tauc J, Grigorovici R, Vancu A. Optical properties and electronic structure of amorphous germanium. Physica Status Solidi B, Basic Research, 1966, 15(2): 627–637
36. Gurin V, Alexeenko A, Zolotovskaya S, Yumashev K. Copper and copper selenide nanoparticles in the sol-gel matrices: structural and optical. Materials Science and Engineering C, 2006, 26(5-7): 952–955
37. Sakr G B, Yahia I S, Fadel M, Fouad S S, Romčevic N. Optical spectroscopy, optical conductivity, dielectric properties and new methods for determining the gap states of CuSe thin films. Journal of Alloys and Compounds, 2010, 507(2): 557–562
38. Petrovic M, Gilic M, Cirkovic J, Romčevic M, Romčevic N, Trajic J, Yahia I S. Optical properties of CuSe thin films—band gap determination. Science of Sintering, 2017, 49(2): 167–174